Surface and bulk phase behavior of dry and hydrated tetradecanol:octadecanol alcohol mixtures

E. Sloutskin
Physics Department, Bar Ilan University, Ramat Gan 52900, Israel

E. B. Sirota
ExxonMobil Research and Engineering Company, Annandale, New Jersey 08801

H. Kraack, O. Gang,[a] and A. Doerr[b]
Physics Department, Bar Ilan University, Ramat Gan 52900, Israel

B. M. Ocko
Physics Department, Brookhaven National Laboratory, Upton, New York 11973

M. Deutsch[c]
Physics Department, Bar Ilan University, Ramat Gan 52900, Israel

(Received 18 January 2002; accepted 6 February 2002)

Surface freezing was studied in dry and hydrated octadecanol:tetradecanol ($C_{18}OH$:$C_{14}OH$) mixtures, using surface tension and synchrotron x-ray surface diffraction techniques. Even small amounts of admixed $C_{18}OH$ were found to induce surface freezing in $C_{14}OH$, which does not exhibit this effect when pure. The phase diagram of the bulk was measured by calorimetry and bulk x-ray diffraction. Upon increasing the bulk mole fraction of $C_{18}OH$ (ϕ) a sharp increase in the bulk supercooling occurs at $\phi \approx 0.4$ in dry mixtures, while no supercooling was observed for the hydrated mixtures. A simple thermodynamical model based on the theory of s-regular mixtures is shown to account well for the dependence of the surface freezing onset temperature of both dry and hydrated mixtures, and the hydrated bulk's freezing temperature on ϕ. Only a phenomenological description exists for the dry bulk's phase diagram. This study is expected to provide a baseline for the general surface and bulk behavior of long-chain alcohol mixtures. © *2002 American Institute of Physics.* [DOI: 10.1063/1.1465401]

I. INTRODUCTION

Normal alcohols are the simplest of the substituted hydrocarbons. Having the molecular structure $CH_3(CH_2)_{n-1}OH$ (denoted C_nOH in the following) they are almost identical with normal-alkanes $[CH_3(CH_2)_{n-2}CH_3]$, the only difference being the exchange of a H on one terminal methyl group by a hydroxyl OH group. However, this small change breaks the inversion symmetry between the two ends of the molecule and renders it slightly polar. More importantly, it modifies the molecular interactions by allowing the formation of hydrogen bonds between adjacent molecules through their hydroxyl groups, while alkanes interact solely by vdW forces.[1] Both monocomponent alkane and alcohol melts were found to exhibit surface freezing (SF), i.e., the formation, by a first order transition, of an hexagonally packed, quasi-2D solid layer at the liquid–vapor interface at a temperature T_s several degrees above their bulk freezing, T_f.[2–5] The surface-frozen layer in alkanes is a single molecule thick, while in alcohols it is a bilayer, with the OH groups residing at the center of the bilayer and forming hydrogen bonds between the adjacent molecules from the upper and lower monolayers comprising the bilayer.[5,6] SF occurs in alcohols of lengths $16 \leqslant n \leqslant 28$, but, unlike in alkanes, only molecules having an even number of carbons show this effect. This odd–even effect may be related to differences in the orientation of the terminal OH group relative to the molecular axis, which renders the formation of hydrogen bonds unfavorable in odd alcohols.[5] One attempt to explain the occurrence of surface freezing in pure alkanes employed the entropic stabilization of the surface layer by thermal fluctuations of the surface molecules along their long axes, which for bulk molecules are suppressed by neighboring layers.[7,8] Another explanation assigned it to a wetting effect of the liquid layer by a solid monolayer due to a favorable surface energy balance established, over a certain temperature range, among the temperature-dependent entropic terms of the various surface energies involved.[9] For alcohols, a small but non-negligible contribution is also obtained from the hydrogen bonding.[10] For long molecules it has been argued that the entropic reduction of the free energy, due to positional fluctuations along the axis and rotational disorder of the molecular planes, is large enough to stabilize the surface frozen layer. However, as n goes below 16, the reduction in the free energy becomes too small to stabilize the surface frozen layer with respect to the liquid surface phase, and the SF vanishes. The present study shows, among other things, that

[a]Present address: Gordon McKay Lab, Division of Applied Sciences, Harvard University, Cambridge, Massachusetts 02138.
[b]Present address: Continental AG, Jaedekamp 30, D-30419 Hannover, Germany.
[c]Author to whom correspondence should be addressed. Electronic mail: deutsch@mail.biu.ac.il

adding even a small amount of $C_{18}OH$ to the bulk phase of $C_{14}OH$ induces SF in the short $C_{14}OH$ molecules. As previous studies show,[11] it is reasonable to assume that, in general, by mixing molecules of two different lengths it is possible to reach regions in phase space where the temperature ranges of existence $\Delta T = |T_s - T_f|$ are nonzero, and larger than those of the pure components. Moreover, new phases and transitions between them can be discovered by varying the molar concentration (ϕ) of the mixtures and the temperature (T).[12,13] The importance of understanding the behavior of alkane and alcohol mixtures is further enhanced by the fact that in most ''real-world'' situations the alkanes and alcohols do not exist as pure materials, but as mixtures. Thus, the investigation of mixtures and their surface behavior has important implications not only for basic science, but also for applied science and industry.

We have chosen to study the $C_{14}OH$ and $C_{18}OH$ alcohols because their chain lengths are close enough to form a solution in the solid state, yet different enough to be clearly distinguishable by x-ray reflectivity (XR) measurements and by thermodynamical techniques. The surface behavior of mixtures is almost always more complicated than that of the bulk, because of phenomena like prewetting, surface enrichment and surface layering.[14] In this study, the theoretical description of the surface behavior turned out to be simpler than that of the bulk, since in the bulk the existence of kinetic barriers for phase formation renders the dry bulk behavior very complicated from a theoretical point of view. Because of the reduced dimensionality at the surface and the possibility of molecular exchange between the surface and the bulk phases, no kinetic barriers exist for the formation of the surface-frozen phase in alkanes and alcohols.[3,11,15] A significant increase in the temperature range of SF was observed for alcohol surfaces residing in a saturated water vapor atmosphere (denoted hereafter as ''hydrated'' or ''wet'' mixtures), as compared to those residing in a dry atmosphere (denoted ''dry'' mixtures).[5,16] Water intercalation into the center of the SF bilayer varies the hydrogen bonding, and imparts an increased stability to the SF bilayer. Due to an anomalous increase in water solubility in the solid rotator phase as compared to the liquid phase, the hydrated alcohols solidify at higher temperatures than the dry ones, both at the surface[5] and in the bulk.[17] However, the temperature shifts relative to the dry case are not equal for the bulk and the surface, rendering the existence ranges ΔT significantly larger than those in the dry samples. We also find that hydration causes bulk supercooling to disappear. The theory of s-regular binary mixtures[18,19] is used here to account for the behavior of $T_s(\phi)$ in hydrated and dry samples, with only a single fitting parameter: the repulsion energy between $C_{14}OH$ and $C_{18}OH$. The results are further supported by the ϕ-variation of the thickness of the surface frozen layer, d, derived from the XR measurements. The same theory accounts for the behavior of the freezing temperature $T_f(\phi)$ of the hydrated bulk. The behavior of the quasi-2D lattice constant for different molar concentrations and temperatures was investigated by grazing-incidence x-ray diffraction methods, both in dry and hydrated samples. In two of the samples the temperature range of SF was large enough to permit the measurement of the linear expansion coefficient of the surface frozen layer. Calorimetric studies were performed to study the phase diagram of the bulk in thermodynamical equilibrium and under kinetic constraints. The bulk phase diagram was also studied by x-ray powder diffraction for two selected dry bulk mixtures, revealing a significant reduction in the stability of the bulk rotator phase with respect to the liquid as compared to the low-temperature crystalline bulk phase.

II. EXPERIMENT

The structure of the SF bilayer was studied by XR[20] and grazing incidence diffraction[5] (GID). The surface thermodynamics were studied using surface tension[2] (ST) measurements. The bulk phase diagram was studied by calorimetry[21] (Cal) and x-ray powder diffraction[22,23] (XD) techniques. The experimental methods are well documented in the literature.[4,11] Only a brief summary will be given here, concentrating mostly on features peculiar to this study.

A. Samples

Materials, purchased from Aldrich and Fluka were $\geqslant$97% and $\geqslant$99% pure for $C_{14}OH$ and $C_{18}OH$, respectively, and used as obtained. The mixtures were prepared by weighing the required amounts for a total volume of 0.3 cm^3 (ST), 0.7 cm^3 (XR and GID), 0.5 cm^3 (Cal), and 5×10^{-4} cm^3 (XD), heating them well above the melting point of $C_{18}OH$, and stirring vigorously on a hotplate with a magnetic stirrer for $>$15 min. The XD samples, measured directly into thin-walled standard x-ray glass capillaries, were not stirred, but rather left at a temperature $\sim$10 °C above the melting point of $C_{18}OH$ for several hours prior to measurements, to allow for good mixing. For the ST and XR experiments on hydrated alcohols a ring shaped water trough with 2–3 cm^3 of water surrounded the alcohol container residing inside the sample cell. This generated a saturated water vapor atmosphere in the cell. Thus, the sample was hydrated by absorbing water from the vapor. A complete restitution of all properties measured on the dry sample was observed upon drying of the hydrated samples.

B. Surface-tension measurements

The ST measurements were performed by the Wilhelmy plate method,[2,11,24] using filter paper plates to enhance wetting by the sample.[25] The computer-controlled experimental setup, including the sample cell, is described in detail in Refs. 2, 4. The ST was measured in discrete temperature steps of 0.05 °C, staying at each temperature step for 30 s. This yields an effective scan rate of 0.1 °C/min. Slower scan rates, and changing the scan direction, did not alter the results, provided that bulk freezing was not reached. Because of unavoidable random variations in cutting the paper plates to size, and in their depth of immersion into the sample melt, the absolute values of the surface tension can be trusted only to $\sim$1 mN/m. However, the relative values within one scan show a significantly smaller scatter, estimated to be $\leqslant$0.05 mN/m.

C. Surface x-ray measurements

The surface-specific x-ray measurements were carried out at the Harvard/BNL liquid surface diffractometer at beamline X22B, National Synchrotron Light Source, Brookhaven National Laboratory, using x rays of wavelength 1.57Å.[4,5,11] The cell, its temperature control, the diffractometer, and the measuring and data analysis procedures have been previously described.[4,5] The density profile of the vapor–liquid interface was studied by x-ray reflectivity[5] (XR) and the surface-parallel structure by grazing incidence diffraction[26] (GID) and Bragg rod measurements[5,6,26] (BR) measurements. The expressions employed for the BR analysis of the bilayer structure were presented elsewhere.[5]

D. Bulk calorimetry

The calorimeter was described in Ref. 21. Relative heat capacities were measured by scanning the temperature at a rate of ~0.1 °C/min rate. The temperature was scanned keeping a constant ~2 °C difference between the sample and the controlled thermal bath. The inverse derivative of the sample temperature versus time is, then, proportional to the heat capacity.[27] No absolute calibration of the heat capacity was done, since the purpose of our calorimetric measurements was to obtain only the temperatures of the phase transitions. These were indicated by peaks in the $(dT_{\text{sample}}/dt)^{-1}$ curve, where t denotes time. While for the pure alcohols the peaks were very sharp, in some of the mixtures very small and broad melting peaks were observed. For an independent detection of the occurrence of phase transitions, a small combined infrared source/detector device[28] was placed above the sample. The sample was placed into a glass container, below which a small piece of black paper was placed. No significant changes in the operation of the calorimeter were observed with and without the glass container and IR sensor. The IR radiation back-reflected into the detector was negligible due to the strong absorption of the black paper, as long as the interposed sample was liquid, and thus transparent. Upon solidification into a white solid, the signal back-reflected into the detector was strongly enhanced. Thus, whenever the melting peaks in the $(dT_{\text{sample}}/dt)^{-1}$ curve were not sharp and strong enough to determine the transition temperature, the point at which the back-reflected intensity was abruptly reduced was designated as the melting temperature. Hydration of the calorimetry samples was done by inserting a ~0.5 cm^3 open Teflon trough filled with water inside the calorimeter's sample cell. In the temperature ranges relevant for this study, the calorimetric signal from such a water container is constant, and thus had no influence on the measured relative heat capacities measured. Since the sample cell is tightly closed, less than 0.5 g of water were enough to establish a saturated water vapor atmosphere. The reflective infrared sensor was not used with the hydrated samples.

E. Bulk x-ray diffraction

Bulk diffraction experiments were carried out on a standard Huber two-circle diffractometer using Cu K_α radiation and a Rigaku 18 kW rotating anode x-ray generator.[23,29] The powder samples were held in sealed standard 2 mm diam quartz capillaries, of 0.01 mm wall thickness. The temperature was scanned in steps of 1 °C, so that the accuracy of the phase transition temperatures observed by the XD method is ±0.5 °C. The samples' temperature was controlled to ≤0.1 °C at any given temperature.

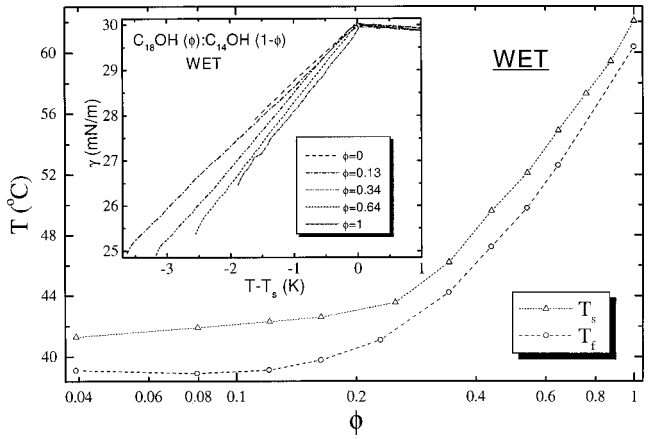

FIG. 1. The (temperature, concentration) phase diagram of the $C_{14}OH$:$C_{18}OH$ hydrated mixtures. T_s was obtained from the ST measurements and the T_f was measured by bulk calorimetry. The freezing and the melting bulk curves coincide, indicating an absence of supercooling for the wet samples. The lines are only a guide to the eye. Several typical ST scans for the $C_{18}OH$ concentrations listed are shown in the inset. The curves end at the bulk freezing temperature T_f. The SF existence range $\Delta T = T_s - T_f$ is observed to be significantly greater for the mixtures, compared to the pure samples. Since the measurement errors in the absolute surface tension values are no better than ~1 mN/m, all curves were shifted by small amounts to make them coincide at T_s to enhance presentation clarity.

III. RESULTS AND DISCUSSION

A. Phase diagrams

Typical ST scans $\gamma(T)$ for different molar concentrations are shown in the inset to Fig. 1. The most outstanding feature of these curves is the slope change, upon cooling, from a negative to a positive value as the surface-frozen layer is formed at $T = T_s$. The surface tension is a direct measure of the surface excess entropy,[2,11] since $d\gamma/dT = -(S_s - S_b)$, where S_s and S_b are the entropies of the surface and of the bulk, respectively. For $T > T_s$, the liquid surface is less ordered than the bulk, as for ordinary liquids, and the slope of $\gamma(T > T_s)$ is negative. For $T < T_s$ the surface phase is ordered, while the bulk remains liquid. Thus, $S_s < S_b$ and the slope of $\gamma(T < T_s)$ is positive. The surface entropy loss upon SF (per unit area) can be calculated as $\Delta S = d\gamma/dT|_{T<T_s} - d\gamma/dT|_{T>T_s}$. The temperature range of existence of the surface-frozen layer, $\Delta T = T_s - T_f$, is terminated at the bulk freezing temperature T_f. The scans shown in the inset were measured for the *hydrated* $C_{18}OH$:$C_{14}OH$ mixtures. $\phi \equiv N/(N+M)$, where $N(M)$ is the number of moles of $C_{18}OH$($C_{14}OH$) in the mixture. Noting the ϕ-trend of the low termination point of $\gamma(T)$ in the inset of Fig. 1, ΔT is clearly seen to be much greater for the mixtures than for the pure alcohols. While the slope of $\gamma(T)$ above T_s stays constant with ϕ, the slope below T_s grows with ϕ. This is not surprising, considering that the entropy loss upon crystallization of an alkyl chain is roughly proportional to the chain

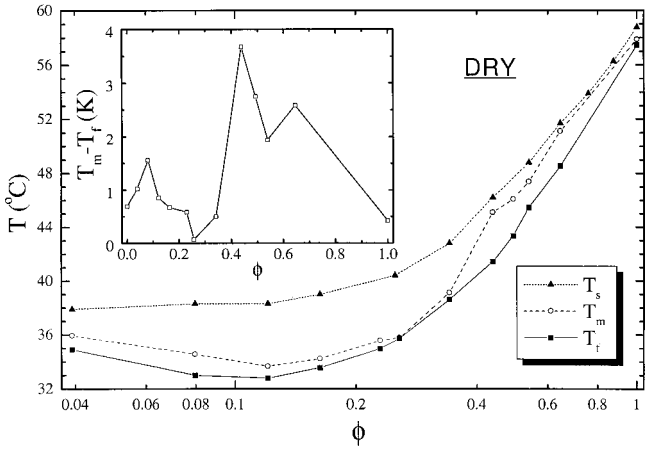

FIG. 2. Same as Fig. 1, but for the dry mixtures. The bulk melting temperatures, T_m (circles), are shown, since finite bulk melting/freezing hysteresis is observed for the dry bulk samples. The significant nonlinearity of the graphs on a logarithmic scale indicates a solid phase mixture behavior, rather than an ideal solution one. The amount of bulk supercooling, $\delta T_{SC}=T_m-T_f$ is shown in the inset. While for $\phi<0.4$ the melting and the freezing temperatures almost coincide, a large hysteresis is observed for samples with $\phi>0.4$.

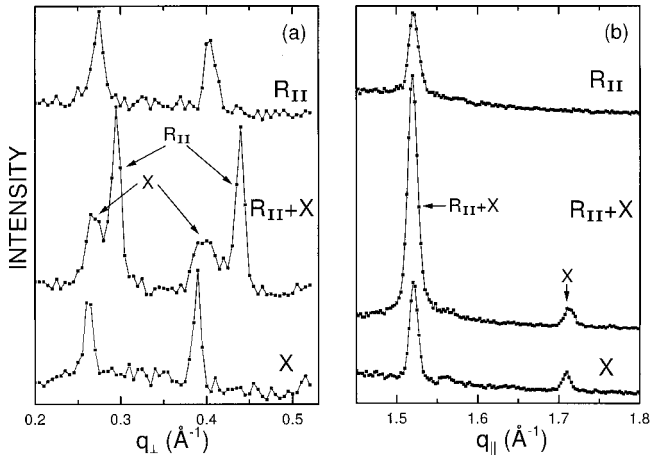

FIG. 3. X-ray bulk diffraction scans for $\phi=0.49$ for different temperatures and phases. (a) Longitudinal (layer-normal) scans $(00l)$. The 002 and 003 peaks are shown. The mixed rotator-crystal $(R_{II}+X)$ phase is easily distinguished from the other two phases as it has four diffraction peaks corresponding to two different coexisting layer spacings. Notice that the rotator (R_{II}) peaks are significantly upshifted in $q_\perp$ for the $R_{II}+X$ mixed phase. (b) Transverse (in-plane) scans. The orthorombic crystalline (X) phase is indicated by the two different in-plane peaks, degenerating into a single in-plane peak for the hexagonal R_{II} phase.

length[2,4] and thus the entropy loss is greater for a greater fraction of the longer component. A more quantitative description of the behavior of $\Delta S(\phi)$ is presented below.

Figure 1 shows the ϕ-variation of T_s (upper line) and T_f (lower line) of the *hydrated* $C_{18}OH$:$C_{14}OH$ mixtures. The melting curve, $T_m(\phi)$, coincides with $T_f(\phi)$ due to the absence of kinetic barriers for solid nucleation in the bulk of hydrated $C_{18}OH$:$C_{14}OH$ mixtures. A similar behavior is obtained for the T_s (upper line) and T_f (lower line) lines of the *dry* mixtures in Fig. 2. Here, however, a distinct melting curve, $T_m(\phi)$, is observed above the $T_f(\phi)$ line indicating that in the absence of water molecules in the samples, a finite supercooling of the bulk liquid becomes possible, i.e., a kinetic barrier to bulk crystallization is established. The $T_{m,s,f}(\phi)$ curves, shown on a semilogarithmic scale, are clearly nonlinear, indicating that the ideal solution theory is not applicable in this case.[11,15] While for the C_{18}:C_{14} alkane mixtures, one might expect a phase separation to occur in the solid state,[30] the hydrogen bonds cause the components in our system to mix well both in the liquid and in the solid phases, despite the chain length mismatch, thus causing the nonlinearity observed. The ϕ-variation of the bulk supercooling, $\delta T_{SC}=T_m-T_f$, is shown in the inset of Fig. 2. Two regimes are observed in the supercooling, with a sharp transition between the two at $\phi\approx0.4$; for $\phi<0.4$ very small bulk hysteresis is observed, while for $\phi>0.4$ bulk supercoolings of more than 3 °C are measured. The structural analysis of the bulk, presented below, shows the microscopic origins of both the supercooling and the nonsupercooling regimes in our systems.

B. Bulk structure

To elucidate the apparent transition from strong ($\phi>0.4$) to weak ($\phi<0.4$) supercooling at $\phi\approx0.4$ in dry mixtures from a microscopic point of view, bulk XD experiments were performed below ($\phi=0.125$) and above ($\phi=0.49$) the transition. Alcohols form lamellar crystals, where each lamella consists of a bilayer of alcohol molecules. For $\phi=0.49$ the XD patterns shown in Fig. 3 consist of several peaks resulting from the lamellae-normal (longitudinal, denoted $q_\perp$) order at small momentum transfer q values, and peaks resulting from the lamellae-parallel (transverse, $q_\parallel$) order at larger q values. Three different ordered phases were found for this ϕ, distinguished by their longitudinal and transverse patterns. The first is a rotator R_{II} phase.[29] This phase consists of ABC stacked bilayers, with molecules aligned along the layer-normal and hexagonally packed in-plane. The molecular centers of mass have long range in-plane positional order but the rotations of the molecular planes about the long axis of the molecules are not correlated, hence the name rotator. The hexagonal packing is reflected in the single transverse peak in Fig. 3(b). Figure 3(a) shows two orders, 002 and 003, of the longitudinal peaks. At low temperatures a crystalline phase appears, denoted here as X, where long-range order is also established in the rotational order of the molecular planes. This has an orthorhombic structure, distinguished by two transverse peaks [Fig. 3(b)]. A two-phase rotator+crystal regime denoted $R_{II}+X$ is observed at intermediate temperatures. Its diffraction pattern consists of the sum of the individual X and R_{II} patterns, as shown in the center lines in Fig. 3. For $\phi=0.125$ only the R_{II} and X phases are found, but not the two-phase state.

The longitudinal $\phi=0.49$ patterns in Fig. 3(a) show that the rotator peaks in the $R_{II}+X$ mixed two-phase region are shifted to a significantly higher $q_\perp$ than the rotator peaks in the pure R_{II} phase. Since for the bulk bilayer spacing (d_b) we have $d_b=m*(2\pi/q)$, where $m=3$ for the 003 peaks, the upshift in $q_\perp$ means that the thickness of the rotator bilayer, which is 46.9 Å in the pure R_{II} phase, is reduced by the presence of the crystal phase to a thickness of only 43.1 Å. This reduction is due to the fact that the compositions of the two phases in the two-phase regime are different from the

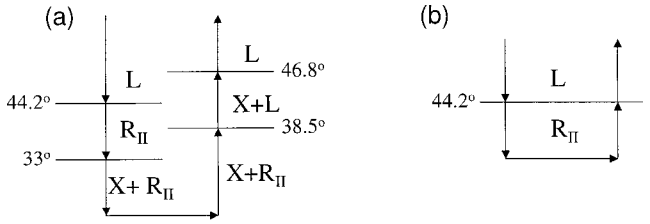

FIG. 4. Schematics of the bulk phase sequence vs temperature as detected by the XD experiments for $\phi=0.49$. The accuracy of all temperatures is ± 0.5 °C. (a) The sample is cooled down below the temperature of crystal (X) nucleation (33 °C). The final melting of such sample, when heated, occurs only at 46.8 °C. (b) The sample is cooled down to the rotator (R_{II}) phase only. Heating of such a sample leads to melting already at 44.2 °C. Notice that the rotator phase melts at 38.5 °C in the presence of the crystal phase (a), while the pure rotator (b) melts only at 44.2 °C.

average, nominal composition. The R_{II} phase in this regime contains an above-nominal fraction of $C_{14}OH$ molecules, which reduces the bilayer's thickness and, as we discuss below, also its melting temperature relative to those of the pure R_{II} phase. A careful comparison of the middle and lower curves in Fig. 3(a) reveals a small shift of the X phase peaks in the mixed regime to a higher $q_\perp$ as compared to those of the pure X phase. This, in turn, indicates that the bilayer in the X phase of the two-phase regime is thinner than the bilayer in the pure X phase. The difference originates, again, in the admixture of $C_{14}OH$ molecules in the X phase in this regime, which reduces the concentration-averaged molecular length. The fact that the reduction of the X phase's average length is smaller than that occurring in the R_{II} phase in this regime indicates that the $C_{14}OH$ concentration is considerably higher in the R_{II} phase than in the X phase in this regime. From the transverse peak position in Fig. 3(b) the area per molecule in the pure R_{II} phase is 19.7 ± 0.2 Å^2 and in the crystalline phase is only 18.4 ± 0.2 Å^2. A similar increase of the molecular area in the rotator phase was observed earlier and was assigned to the proliferation of gauche conformations at the chain ends in the rotator phase.[17,23] Note that the length increase of the pure X phase relative to the pure R_{II} phase does not compensate for the molecular area reduction, so that the molecular volume in the pure X phase is about 5% smaller than that in the pure R_{II} phase.

The phase sequence observed with variation of the temperature for the $\phi=0.49$ mixture is schematized in Fig. 4. Cooling from the melt, an R_{II} rotator phase was found to exist below the liquid phase (L), with a freezing transition at 44.2 °C. Upon further cooling a segregation occurs at 33 °C to a two-phase region with a rotator R_{II} and an orthorhombic crystal (X) phases, as shown schematically in Fig. 4(a). Upon heating up from this two phase $R_{II}+X$ regime, a transition to an $X+L$ phase occurs at 38.5 °C, with the X phase remaining stable up to 46.8 °C, i.e., ~2.6 °C above the liquid-to-rotator freezing temperature T_f. While the segregated $X+L$ has a lower free energy at that temperature, the mixed metastable rotator phase with a low nucleation barrier is stable with respect to the liquid. Finally, as shown in Fig. 4(b), heating up from the R_{II} phase leads to a melting ($R_{II}-L$) transition at $T=T_f=44.2$ °C, i.e., no supercooling is observed: $\delta T_{SC}=0$.

TABLE I. Thermodynamical data obtained by ST and Cal measurements for different $C_{18}OH$:$C_{14}OH$ mixtures. ϕ is the bulk mole fraction of $C_{18}OH$, T_s and T_f are the surface and the bulk freezing temperatures, respectively, and T_m is the bulk melting temperature. ΔS is the entropy change upon surface freezing, as obtained from the slopes of the $\gamma(T)$ curve above and below T_s.

	Dry mixtures				Hydrated mixtures		
ϕ Mole fraction	T_s (°C)	T_m (°C)	T_f (°C)	ΔS_{DRY} [mJ/(m^2 K)]	T_s (°C)	T_f (°C)	ΔS_{WET} [mJ/(m^2 K)]
1	58.8	57.9	57.4	2.07	62	60.3	1.9
0.88	56.2			2.09	59.4	57.4	1.89
0.76	53.9			2.09	57.3	55	1.86
0.64	51.7	51.1	48.5	2.04	54.9	52.3	1.87
0.54	48.8	47.4	45.5	2.01	52.1	49.4	1.79
0.49		46.1	43.3				
0.44	46.2	45.1	41.4	1.89	49.6	46.7	1.79
0.34	42.8	39.1	38.6	1.88	46.2	43.1	1.77
0.25	40.4	35.8	35.7	1.81	43.6	41	1.62
0.23		35.6	35				
0.16	39	34.2	33.6	1.67	42.6	38.9	1.48
0.12	38.3	33.6	32.8	1.59	42.3	38.7	1.44
0.08	38.3	34.6	33	1.51	41.9	38.8	1.39
0.04	37.9	35.9	34.9	1.49	41.3	38.7	1.35
0		37.2	36.5		41.1	39.4	1.3

The $\phi=0.125$ mixture presents a simpler sequence. An R_{II} phase is nucleated at $T_f=33.1\pm 0.5$ °C. This rotator phase converts (in $\lesssim$24 h) at room temperature to an X phase. This is an example of a transient rotator phase induced nucleation with subsequent conversion to the crystal phase, as seen in alkane melts and solutions.[31] On heating from this X phase, melting occurs close to the freezing from the liquid to the rotator, i.e., $T_m=33.1\pm 0.5$ °C. The more accurate calorimetry measurements reveal a supercooling of ~0.8 °C for this mixture, as listed in Table I.

In conclusion, the XD results show the ϕ-dependent trends in the supercooling δT_{SC} of the dry $C_{18}OH$:$C_{14}OH$ mixture, observed in Fig. 2, to originate not in a conventional supercooling scheme such as found previously for alkane melts[21] and solutions,[11] but rather in a complicated interplay between four different bulk regimes: a rotator, a crystal, their mixture, and a liquid, and their temperature ranges of stability.

C. Surface structure

1. Surface-normal structure: Dry samples

The surface-normal structure was studied by XR measurements. Figure 5 shows the XR curves (points) for different compositions of $C_{18}OH$:$C_{14}OH$, the theoretical fits (see below) are shown in lines, and the corresponding surface-normal density profiles are given in the inset. Here $q_z=(4\pi/\lambda)\sin\alpha$, is the momentum transfer perpendicular to the surface, where α is the incidence angle relative to the surface and λ is the wavelength of the x rays. For each concentration, the reflectivity is shown above $T_s(\phi)$ (when the surface layer is liquid) and in the surface-frozen regime. Typically for liquid surfaces,[20,26] the curves measured above $T_s(\phi)$ decrease monotonically with q_z. As can be seen by the fitted lines, they are well described by

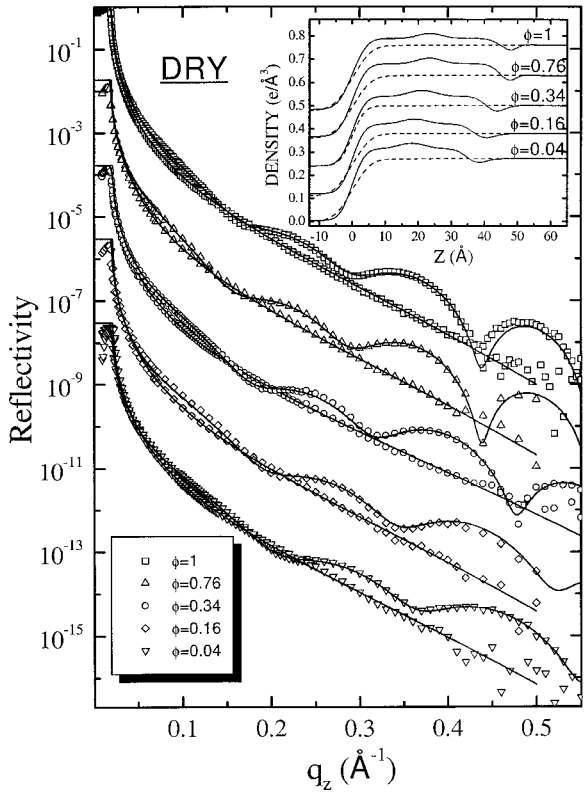

FIG. 5. Measured (points) x-ray reflectivities for dry samples of the concentrations indicated in their liquid surface phase (monotonically decreasing curves) and in the surface crystalline bilayer phase (modulated curves). The solid lines are fits using the model density profile for the surface crystalline bilayer discussed in the text. The surface-normal electron density profiles corresponding to the fits, for the crystalline (solid) and liquid (dash) surface phases are shown in the inset. Reflectivity and density curves are shifted for clarity.

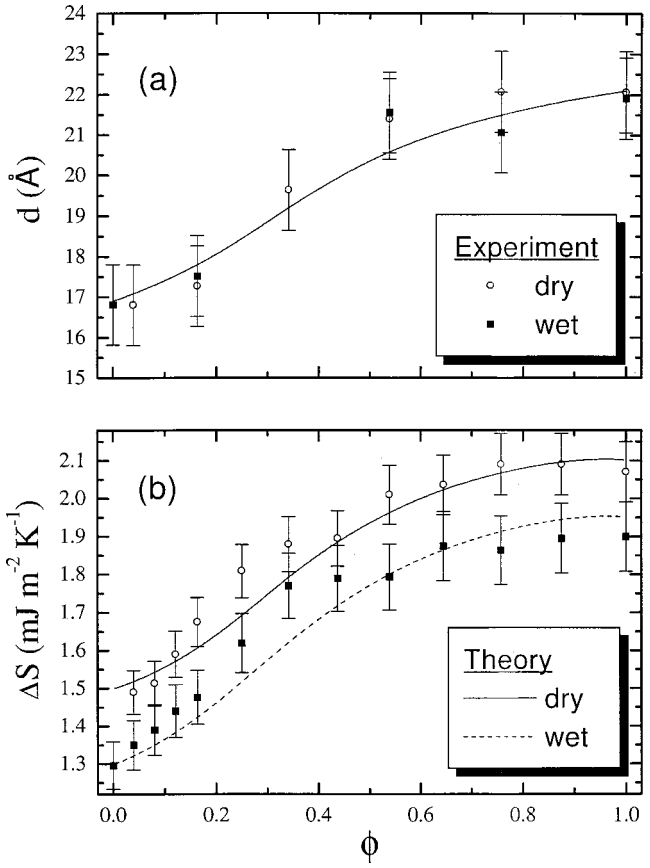

FIG. 6. (a) Thickness of the alkyl slab of the surface frozen layer, as derived from the measured reflectivity fits of dry (open circles) and wet (solid squares) $C_{18}OH$:$C_{14}OH$ mixtures. The theoretical thickness calculated from the fits to phase diagrams (Fig. 10) of the wet and the dry mixtures are indistinguishable on the scale of the figure, and are shown by the single line. (b) The entropy loss upon surface freezing obtained from the ST measurements (points). The wet ΔS values (solid squares) are lower than the dry ones (open circles) due to remnant ordering in the liquid phase. The theoretical ΔS calculated from the fits to phase diagrams are shown in a solid line for the dry mixtures and by a dashed line for the hydrated ones.

$$R(q_z)=\left|\frac{q_z-\sqrt{q_z^2-q_c^2}}{q_z+\sqrt{q_z^2-q_c^2}}\right|^2 \exp(-q_z^2\sigma^2), \qquad (1)$$

where q_c is the surface-normal momentum transfer at the critical angle for total reflection, α_c. The fraction appearing in this expression is the well-known Fresnel reflectivity, $R_F(q_z)$, and the exponential factor arises from the Gaussian-distributed surface roughness σ.[20,26] This roughness is mainly due to thermally excited capillary waves.[32] Below T_s, Kiessig-type fringes are observed in the reflectivity curve, indicating the appearance of a surface layer of a density different from that of the bulk. The period of the fringes is indicative of the layer's thickness, and the fringe contrast—of the difference in electron density between the bulk and the surface layer. The reflectivities in the surface crystalline phase are analyzed quantitatively using a layered interface (''box'') model. This model consists of four slabs: (1) the $(CH_2)_{n-1}$ chain of the upper layer; (2) the OH head groups region; (3) the $(CH_2)_{n-1}$ chain of the lower layer [same as box (1)]; and (4) the innermost CH_3 terminal group. An additional box represents the liquid subphase. This is the same model that was successfully used previously to model the surface frozen layer of pure alcohols.[5,6] Three different roughness parameters were assumed: (1) at the vapor interface and above the CH_3 groups slab; (2) at the interfaces of the OH groups slab; (3) at the layer-liquid bulk interface. In the inset, the dashed lines ($T>T_s$) represent a simple, continuous liquid–vapor interface, broadened by capillary wave roughness. The solid lines ($T_f<T<T_s$) demonstrate the existence of a high-density region above the liquid bulk phase.

The thickness d of the alkyl slabs [box(1)=box(3)], as obtained from the fit for the different ϕ, is shown in Fig. 6(a) (open circles). A clear growth with increasing ϕ is observed in this quantity, as a larger fraction of the long chains is incorporated into the surface frozen layer. Although d as derived from XR is not sensitive to small molecular tilts, the layer thicknesses obtained indicate that the molecules are untilted with respect to the surface normal, as expected for these low n molecules.[5] A good quantitative description, shown by a line, of the variation of d with ϕ is obtained from the thermodynamical theory presented below. Since the OH and the CH_3 slabs' thicknesses do not change with ϕ, the overall thickness of the layer also grows, as is seen in the inset to Fig. 5. The measurements clearly show that at $\phi=0.04$ the thickness of the surface frozen layer is equal to $C_{14}OH$ bulk rotator bilayer thickness. This means that in

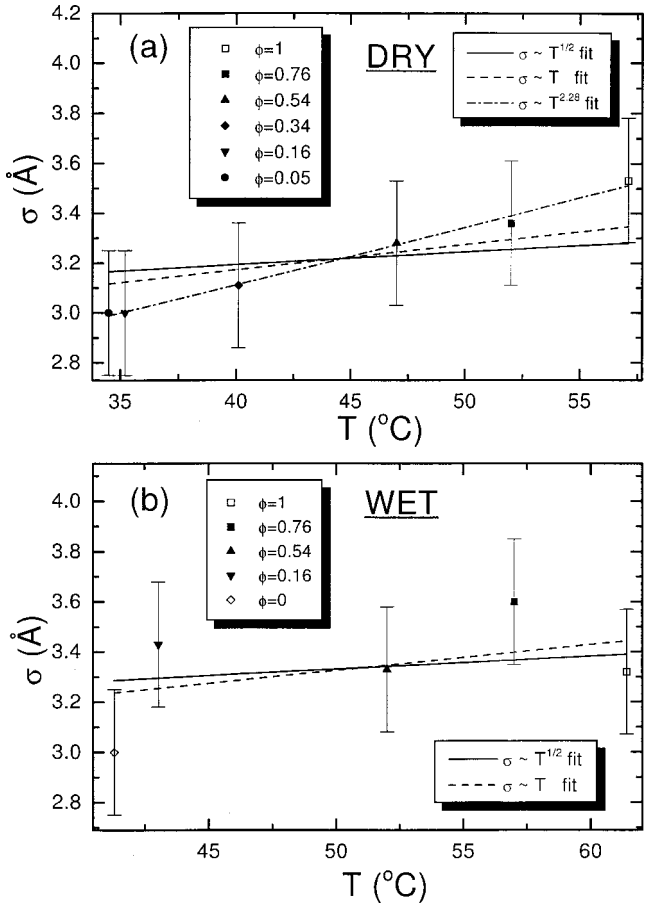

FIG. 7. Surface roughness $\sigma(\phi)$ values for (a) dry and (b) wet mixtures derived from fits to the measured reflectivity. The slight increase in σ with ϕ is due to the corresponding increase in the temperature. The lines are fits to standard capillary-wave theory (solid line) and the entropic theory of surface freezing of Tkachenko and Rabin (Refs. 7, 8) (dashed line). In (a) the best fit to a T^b form is also shown (dashed–dotted line). This fit yields $b \approx 2.28$.

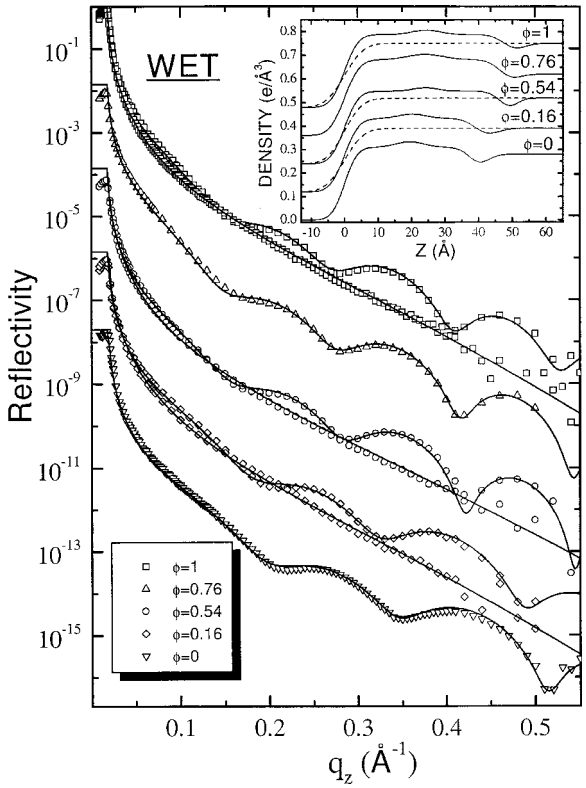

FIG. 8. Same as Fig. 5, but for hydrated mixtures. Note the increase in the OH region thickness in the inset as compared to the dry mixtures.

the presence of a small $C_{18}OH$ fraction in the bulk phase, the $C_{14}OH$ molecules tend to exhibit a SF effect, in contrast with pure $C_{14}OH$, which does not exhibit SF.[5] The density of the surface frozen $(CH_2)_{n-1}$ chains is obtained from the fit as $0.304 \pm 0.006\, e/Å^3$, equal, within the combined experimental error, to the value obtained for pure alcohols,[5,6] and somewhat lower than the $0.321\ e/Å^3$ obtained for the pure alkanes.[4,11] The density of the alkyl chains in the surface frozen solid, as derived from the XR measurements, is higher by ~13% than the density of the bulk liquid, and is equal to that of the bulk rotator phase,[1] indicating a full coverage of the liquid surface by the bilayer. The thicknesses of the OH and CH_3 slabs were set to 2.5 Å and 2.3 Å, respectively, which are the values obtained for the pure materials.[5]

The roughness $\sigma(T)$ at the bilayer-vapor interface is plotted in Fig. 7(a). The variation of this quantity with T (through the variation of ϕ) is, in principle, of great importance, since one of the measurable predictions of the Tkachenko–Rabin (TR) theoretical model[7,8] for the formation of the SF effect is an anomalous, $\sigma(T) \sim T$, functional dependence rather than the conventional $\sigma(T) \sim T^{1/2}$ dependence, predicted by capillary wave theory (CWT). As Fig. 7(a) shows, the temperature range of the effect in our case is too small for unambiguously differentiating between these two functional forms, even if σ can be assumed to be independent of ϕ and dependent only on T. As one can see from the plot, the CWT (solid line) and TR (dashed) models predictions are both inside the error bars, while a phenomenological power law fit yields a $T^{2.28}$ dependence (dashed–dotted), which does not correspond to either of the existing theories.

2. Surface-normal structure: Wet samples

Figure 8 shows the measured (points) and fitted (lines) XR of the wet mixtures, with the corresponding density profiles shown in the inset. The general behavior is similar to that observed for the dry samples (above). At $T > T_s$ a usual liquid–vapor interface behavior is observed, showing a monotonic decrease in the reflectivity. The surface frozen samples ($T < T_s$) show Kiessig fringes in the $R(q_z)$ curves. The alkyl group lengths d derived from the fits [Fig. 6(a)] are equal, to within their error bars, to those obtained for the dry samples. As d is a weighted average of the alkyl group lengths of the two components, the equality of the derived d values in the wet and dry cases indicates that hydration does not significantly influence the composition of the surface bilayer. The main difference between the profiles obtained in the fits here and the ones obtained for the dry samples is that here the thickness of the OH-groups slab had to be increased by almost 3 Å to obtain a good fit. This change is assigned to the intercalation of water molecules in the middle of the bilayer, as observed previously for hydrated pure alcohols.[5,16] The density of the surface frozen $(CH_2)_{n-1}$

chains is found to be here $0.310\pm0.006\ e/\text{Å}^3$, equal, within the combined experimental error, to the value obtained for the dry mixture. The OH slab's density is $0.35\pm0.01\ e/\text{Å}^3$ also equal, within the combined errors, to that of the dry sample, $0.38\pm0.02\ e/\text{Å}^3$. The bulk-bilayer interface roughness stays constant at 3.2 ± 0.5 Å and the OH-slab roughness stays constant at 4.1 ± 0.5 Å for all T and ϕ. The bilayer–vapor interface roughness, σ, is shown in Fig. 7(b). As for dry samples, the T-range spanned by the ϕ-range is too small to allow a meaningful distinction between the TR (dashed) and the CWT (solid line) predictions.

3. Surface-parallel structure

To probe the structure within the surface plane, grazing incidence diffraction measurements were carried out. The in-plane full width at half maximum resolution of these measurements, achieved by using Soller collimators, was $\Delta q_\parallel \approx 6\times10^{-3}$ Å^{-1}, except for the pure $C_{18}OH$ where a coarser resolution of $\Delta q_\parallel \approx 3\times10^{-2}$ Å^{-1} was employed. Typical GID scans for $\phi=0.16$ at different temperatures are shown in Fig. 9(a), using triangles for the dry mixtures and squares for the wet ones. For all samples, a single in-plane peak was observed at $q_\parallel \approx 1.46$–1.5 Å^{-1}, indicating a hexagonal packing within the surface plane, as found for pure alcohols (with the possible exception of $C_{28}OH$),[5] alkanes[4] of lengths $n \leqslant 30$ and alkane solutions.[11] The peak position corresponds to a nearest-neighbor chain separation in the surface plane of $a=2\pi/[q_\parallel \cos(30°)] \approx 4.8$–$5$ Å for our case of hexagonal packing. Figure 9(b) displays the values of a for different temperatures and concentrations with dry mixtures denoted by open symbols, the wet mixtures by solid ones. While for the pure materials a significant increase in a is observed upon hydration,[5] the nearest-neighbor separation in the mixtures is only slightly dependent on hydration, if at all, as observed in Fig. 9(b). A similar very weak dependence of the lattice spacing on hydration was found for both pure and mixed bulk alcohol samples.[17] The effect observed here is probably due to the amount of voids in the ordered different-lengths chains, which is large enough to accommodate the H_2O molecules without distorting the lattice structure. For $\phi=0.16$ the temperature existence range of SF was large enough ($\sim$4 °C) to permit for linear thermal expansion coefficient $[(da/dT)/a]$ to be measured. The values obtained are $(1.02\pm0.05)\times10^{-3}\,°\text{C}^{-1}$ and $(1.16\pm0.17)\times10^{-3}\,°\text{C}^{-1}$ for the dry and the wet SF bilayers, respectively. These values are somewhat greater than the $(6\pm0.5)\times10^{-4}\,°\text{C}^{-1}$, obtained previously for the dry and hydrated R_{II} bulk phase in pure and mixed alcohols,[17] and the $(6.5\pm0.5)\times10^{-4}\,°\text{C}^{-1}$ measured for a surface-frozen C_{23} monolayer of a C_{23}:C_{12} solution.[11] A similar $(9\pm0.5)\times10^{-4}\,°\text{C}^{-1}$ was also found for the surface frozen layer of a pure C_{20} alkane.[33] Our values are also close to the $\sim1.15\times10^{-3}\,°\text{C}^{-1}$ of the R_{I} bulk phase in pure alkanes[29] but are significantly higher than the $\sim2.6\times10^{-4}\,°\text{C}^{-1}$ obtained for the bulk herringbone orthorhombic crystalline phase in alkanes.[29]

The area per molecule in the frozen surface layer is obtained from the x-ray measurements as $A=8\pi^2/(\sqrt{3}q_\parallel^2)$, which, for our data, varies from 20.2 Å^2 for dry $(\phi,T)=(0.16,34.5\,°\text{C})$ to 21.4 Å^2 for wet $(\phi,T)=(0,41.3\,°\text{C})$. The resultant electron density of the alkyl chain, having 8 electrons per CH_2 group and a projected length of 1.27 Å along the molecular axis, can be estimated directly as $8/(20.16\times1.27)=0.312\ e/\text{Å}^3$ and $8/(21.4\times1.27)=0.294\ e/\text{Å}^3$ for the two extreme areas. Since the reflectivity (XR) experiments probe the macroscopic x-ray illuminated area, while the GID probes only the ordered regions, the fact that the GID values are even lower than those obtained from the XR strongly supports the conclusion that the surface is fully covered by the ordered bilayer. A complete coverage of the surface by the surface layer was also found for the pure alkanes[4] and alcohols,[5] while in some of the alkanes' solutions an incomplete coverage was observed.[11] The widths of the GID peaks were resolution limited, implying in-plane coherence lengths of several thousands Å. While the sharp x-ray peaks clearly prove

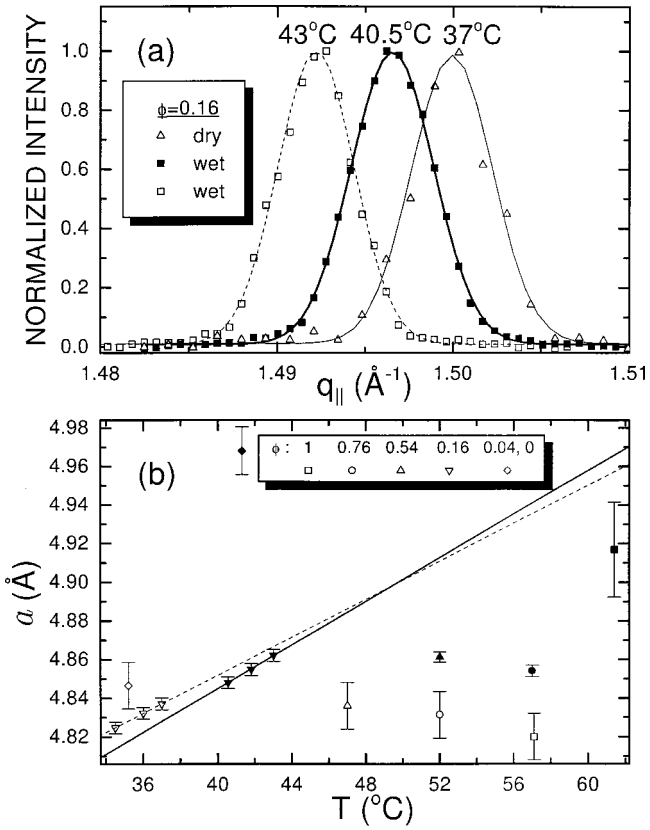

FIG. 9. (a) Measured GID peaks (points) of the surface-frozen bilayer at $\phi=0.16$, and fits by a single Lorentzian (lines). The shift in position with temperature is clearly observed. The left peak (triangles) was measured for the dry sample, while the other two (squares) are for the hydrated one. (b) The nearest-neighbor chain separation in the surface plane a, derived from the GID measurements for the various dry (open) and wet (solid) mixtures and temperatures. In dry $C_{14}OH$ there is no SF, thus the open diamonds are used for the dry $\phi=0.04$ mixture, while the solid diamond denotes the hydrated pure ($\phi=0$) $C_{14}OH$, which does exhibit SF. The pure hydrated materials exhibit considerably larger lattice constant than all other samples, showing that the intercalation of the water molecules into the pure material lattice causes significant strains, while in the mixed lattice the voids are big enough to allow for water incorporation without causing changes in the lattice constant. For the $\phi=0.16$ samples (both dry and wet) the three different-temperature points allow deriving the linear thermal expansion coefficients of $(da/dT)/a=(1.02\pm0.05)\times10^{-3}\,°\text{C}^{-1}$ and $(1.16\pm0.17)\times10^{-3}\,°\text{C}^{-1}$ for the dry and the wet mixture, respectively.

the existence of quasi-2D order in the surface frozen bilayer, our finite resolution does not allow for a detailed line shape analysis, which could distinguish the manner whereby the in-plane correlations decay with distance.

The Bragg rod (BR) scans for several dry and wet compositions were also analyzed. In all cases a bilayer of untitled molecules was found, corresponding to an R_{II} hexagonal quasi-2D phase, similar to those found for pure alcohols[5] of lengths $n \leqslant 22$ and alkanes[4] of lengths $n \leqslant 30$.

D. Theoretical analysis

To account for the ϕ dependence of T_s in the dry mixtures, we invoke the general thermodynamics of binary mixtures,[18,34] using the properties of the pure components. A somewhat similar approach was used previously for C_{23}:C_{12} alkane solutions.[11]

In the liquid phase, the free energy F^l for a mixture of N moles of $C_{18}OH$ and M moles of $C_{14}OH$ can be written as[18,31,35,36]

$$F^l = N f_{18}^l + M f_{14}^l + k_B T[N \ln(\phi) + M \ln(1-\phi)]. \qquad (2)$$

Here $f_i^l = \epsilon_i - TS_i$, where $i = 18$ or 14 is the free energy of a $C_{18}OH$ or $C_{14}OH$ molecule in a melt of the pure material, S_i is its entropy, and ϵ_i is its internal energy. $\phi \equiv N/(N+M)$ is the mole fraction of $C_{18}OH$ in the bulk liquid. The mole fraction at the surface, ϕ^s, is, in general, not equal to the bulk fraction ϕ and is determined through the simplest form of the well-known Gibbs adsorption rule.[11] In the liquid phase, the two components are assumed to form an ideal mixture, since the chain length mismatch is unimportant in the presence of a large amount of gauche kinks.

The free energy expression of the solid phase is the same as Eq. (2), with two obvious changes. The first change is that the interchange energy term,[18,37] must now be included since with the chains becoming extended the chain length mismatch energy becomes significant. In the zeroth approximation, this extensive nearest-neighbor interchange energy term is $(N^s + M^s)x(1-x)\omega$, where N^s (M^s) are number of moles of $C_{18}OH$ ($C_{14}OH$) in the surface-frozen solid phase, and $x = N^s/(N^s + M^s)$ is the mole fraction of $C_{18}OH$ in the solid surface. ω is the interchange energy per single molecule. It is defined[38] such that if we have two crystals of the pure components, A and B, exchanging an interior A molecule with an interior B molecule will increase the total energy by 2ω. The second change is the obvious replacement of ϕ by x.

Differentiating the free energies to obtain the chemical potentials and using some basic thermodynamics, one gets for the surface a system of two nonlinear equations,[39]

$$T_s(\phi) = \frac{T_{s,18}\Delta S_{18} - \omega(1-x)^2}{\Delta S_{18} + k_B \ln(x/\phi^s)},$$
$$T_s(\phi) = \frac{T_{s,14}\Delta S_{14} - \omega x^2}{\Delta S_{14} + k_B \ln[(1-x)/(1-\phi^s)]}, \qquad (3)$$

which can be solved numerically for the molar fraction in the solid surface phase, $x(\phi)$ and for $T_s(\phi)$, if ω is known. Here $T_{s,18}$ ($T_{s,14}$) and ΔS_{18} (ΔS_{14}) denote the T_s and the ΔS of pure $C_{18}OH$ ($C_{14}OH$), which are measured directly. In the case where several solutions are obtained for $x(\phi)$, the one yielding the highest $T_s(\phi)$ is the physical one. The value of ω is chosen to make the calculated $T_s(\phi)$ values fit the actual values measured by ST, as shown in Fig. 10. Once $x(\phi)$ is obtained, one can go back to the free energy expression Eq. (2) and evaluate the entropy loss upon surface freezing of the mixture. While this theoretical approach is, clearly, an oversimplification of the problem, it describes well the behavior of the experimentally measured thermodynamical quantities. The microscopic theories of SF in pure materials do not contradict the analysis presented here, since recent mixture theory is based on the pure materials' properties, thus taking into account all possible microscopical causes for the existence of SF (be they anomalous solid-phase fluctuations,[7,8,10] wetting effects[9] or other phenomena) up to first order in ϕ.

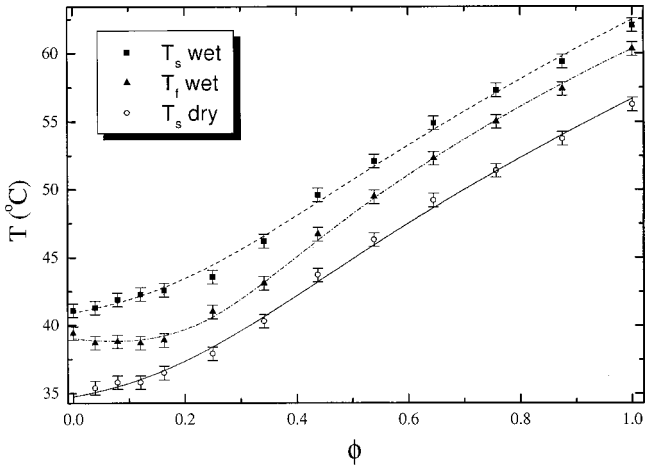

FIG. 10. The theoretical fits (lines) to the dry (solid) and wet (dashed) surface phase diagram, and to the wet bulk phase diagram (dashed–dotted). S-regular mixture theory is used. The measured T_s and T_f data (points) are all taken from ST measurements. The dry surface phase diagram was downshifted for clarity by 2 °C.

For hydrated mixtures, exactly the same system of equations is used, but now the temperatures and the entropies of SF of *hydrated* pure $C_{18}OH$ and $C_{14}OH$ should be used for $T_{s,18}$, $T_{s,14}$, ΔS_{18}, and ΔS_{14}. One can easily show,[39] that this is equivalent to a linear approximation of the water fraction behavior versus ϕ. The *bulk* freezing in hydrated mixtures is also described by the same theory, but now the nominal ϕ should be used instead ϕ^s and the *hydrated* $C_{18}OH$ and $C_{14}OH$ *bulk* freezing temperature $T_{f,18}$ and $T_{f,14}$ should be used instead of $T_{s,18}$ and $T_{s,14}$.

Since no accurate absolute ST values could be obtained with our equipment, we used for the calculation of ϕ^s of both the dry and wet samples literature values of the ST measured for dry samples.[40] Also, since ΔS_{18} and ΔS_{14} values normalized to a single molecule (and not to the molecular area[11]) were required, published calorimetric values for the *dry bulk*[17] were used for all the fits herein.

The fits to the dry (solid line) and hydrated (dashed line) temperatures of surface freezing for the different fractions of $C_{18}OH$ (ϕ), are shown in Fig. 10, along with the fit to the hydrated bulk freezing temperatures (dashed–dotted line). To obtain the $T_s(\phi)$ and $T_f(\phi)$ fits shown in the figure, Eqs. (3) were solved numerically to yield T_s and x for each ϕ value,

while only one fitting parameter, ω, was used for each of the graphs shown. One can see, that despite the clear oversimplifications in our model, a good agreement is achieved between this model and the experimental data. An interchange energy of $\omega \approx 1.9$ kJ/mol was obtained from the fit for the surface of both the dry and the wet mixtures and $\omega \approx 2.7$ kJ/mol was obtained for the wet bulk. These results are of the same order of magnitude as predicted by Matheson[30] for bulk mixtures of C_{14}:C_{18} *alkanes*. However, an exact comparison with Matheson's theory[30] is not possible here, since the surface-normal thermal expansion coefficient needed therein is not known for the surface frozen layer, and the wet bulk bilayer spacing behavior is much more complicated, demonstrating a negative expansion coefficient.[17] Not surprisingly, the interchange energy (or, in other words, the energetic cost of chain mismatch) is smaller by ~30% at the surface, compared to the bulk, as no restrictions by neighbor bilayers are imposed at the vapor interface. The $x(\phi)$ values obtained from the fit in Fig. 10, were used to check also the correspondence of our theory with the behavior of $d(\phi)$, as obtained from the XR fits, and shown in Fig. 6 above. The theoretical line, calculated as $d = 1.3[18x + 14(1-x)]$ is shown in Fig. 6(a), along with the XR fit results (points). The line passes inside the error bar of all XR-derived points. This agreement, without any adjustable parameters strongly supports our simple model. The behavior of $x(\phi)$ is identical for the dry and hydrated samples on our scale, so that only one line is shown for dry and hydrated $d(\phi)$. The same is true for the XR-derived $d(\phi)$, where the alkyl block thicknesses were shown above to be equal (within the combined measurement errors) for the dry and the wet samples. Another check on our theoretical model is done by comparing the results obtained from the $T_s(\phi)$ fit to the $\Delta S(\phi)$ data, obtained from ST experiments as discussed above. The entropy loss upon surface freezing was calculated from the free energy expressions of the solid and the liquid phases, using the $x(\phi)$ values obtained from the $T_s(\phi)$ fit. The results (lines) are shown in Fig. 6(b) along with the measured $\Delta S(\phi)$ values (points). The overall agreement between the no-adjustable-parameter lines and experiment is, again, very good for both wet and dry mixtures, except for some small deviations near $\phi \approx 0.4$. We conclude therefore that the theoretical model presented here accounts well for the observations both at the surface and the wet bulk, in spite of its admittedly simplistic approach.

IV. CONCLUSIONS

We presented here x-ray and surface tension studies of surface freezing, as well as bulk phase diagram measurements by calorimetry and x-ray bulk diffraction, in dry and hydrated $C_{14}OH$:$C_{18}OH$ mixtures. Several important thermodynamical quantities derived from the measurements are listed in Table I for the various concentrations and temperatures studied. Table II provides the structural quantities derived from the GID measurements for the surface-frozen layers. The surface layer is found to consist of a mixture of the two components, despite the differences in their chain lengths. The in-plane structure of the surface layer is found to be hexagonal, with its linear expansion coefficient being close to those obtained for the bulk rotator phases. The hydration does not influence the relative concentrations of $C_{14}OH$ and $C_{18}OH$ in the surface frozen phase, but intercalation of water molecules in the middle of the bilayer increases the overall thickness of the bilayer. Also, the entropy loss upon SF in the hydrated mixtures is smaller than those of the dry ones, possibly due to finite ordering in the liquid phase, induced by the hydrogen bonds formed between the molecules. The temperatures of surface and bulk transitions are shifted up by hydration, since the hydrogen bonds formed in the rotator phase stabilize it with respect to the liquid. Hydration also enhances the bilayer's stability, as manifested in the larger temperature range of existence of the SF phase in hydrated samples relative to those of the dry ones. In the bulk phase, hydration reduces the kinetic barriers for nucleation of the rotator phase from the liquid. By contrast, the phase diagram of the dry bulk is determined to a high degree by the kinetics of the various transitions, thus being difficult to describe quantitatively in terms of equilibrium thermodynamics and statistical mechanics. However, the surface phase diagram of both wet and dry samples and the phase diagram of the wet bulk are shown to follow an s-regular mixture behavior, where the interaction between the different molecules can be considered weak enough to employ the zeroth order approximation in s-regular mixtures theory.[18] The complicated interactions between the OH groups are therefore only slightly modified in a mixture comprising molecules of different chain lengths, as compared to those in the pure materials. This, in turn, allowed us to construct a simple theory, based only on the pure materials' properties. The interchange energy in both dry and wet surface-frozen bilayer is smaller by ~30% than the interchange energy in the hydrated solid bulk, indicating a significant decrease in the interlamellar interactions in the surface layer as compared to those in the bulk phases. This reduced sensitivity to chain lengths mismatches is of the same origin as the increase in long-axis fluctuations at the surface, proposed by TR (Refs. 7 and 8) as the microscopic reason for the surface freezing effect in pure alkanes. While $C_{14}OH$:$C_{18}OH$ was chosen *a priori* to provide a baseline, i.e., a kind of ''standard'' for the behavior of alcohol mixtures, further studies on the surface and bulk properties of

TABLE II. Grazing incidence x-ray diffraction results from measurements on the surface frozen bilayer for various $C_{18}OH$ concentrations (ϕ) and temperatures (T). $q_\parallel$ is the position of the single GID peak observed, and $a = 2\pi/[q_\parallel \cos(30°)]$ is the corresponding in-plane intermolecular distance.

	Dry mixtures			Hydrated mixtures		
ϕ Mole fraction	T (°C)	$q_\parallel$ (Å^{-1})	a (Å)	T (°C)	$q_\parallel$ (Å^{-1})	a (Å)
1	57.1	1.505	4.82	61.4	1.476	4.917
0.76	52	1.501	4.831	57	1.495	4.854
0.54	47	1.5	4.836	52	1.493	4.859
0.16	37	1.5	4.837	43	1.492	4.862
	36	1.501	4.832	41.8	1.494	4.855
	34.5	1.504	4.825	40.5	1.496	4.848
0.04	35.2	1.497	4.846			
0				41.3	1.46	4.968

different alcohol and alkane mixtures and solutions are required to elucidate the behavior of the interchange energy for different chain length mismatches. Obviously, as the chain length mismatch grows, the ability to describe the system in terms of the zeroth approximation in s-regular mixtures theory should diminish, and once the deviations from this simple theory are large enough, the agreement of the experimental data with more advanced theories can be checked.

ACKNOWLEDGMENTS

The authors thank Y. Hobarah (Bar-Ilan University) for expert help with the reflective object sensor, and NSLS for beamtime at X22B. Brookhaven National Laboratory is supported by the U.S. Department of Energy under Contract No. DE-AC02-98CH10886.

[1] M. Small, *The Physical Chemistry of Lipids* (Plenum, New York, 1986).
[2] X. Z. Wu, B. M. Ocko, E. B. Sirota, S. K. Sinha, M. Deutsch, B. H. Cao, and M. W. Kim, Science **261**, 1018 (1993).
[3] X. Z. Wu, E. B. Sirota, S. K. Sinha, B. M. Ocko, and M. Deutsch, Phys. Rev. Lett. **70**, 958 (1993).
[4] B. M. Ocko, X. Z. Wu, E. B. Sirota, S. K. Sinha, O. Gang, and M. Deutsch, Phys. Rev. E **55**, 3164 (1997).
[5] O. Gang, X. Z. Wu, B. M. Ocko, E. B. Sirota, and M. Deutsch, Phys. Rev. E **58**, 6086 (1998).
[6] M. Deutsch, X. Z. Wu, E. B. Sirota, S. K. Sinha, B. M. Ocko, and O. M. Magnussen, Europhys. Lett. **30**, 283 (1995).
[7] A. V. Tkachenko and Y. Rabin, Phys. Rev. Lett. **76**, 2527 (1996).
[8] A. V. Tkachenko and Y. Rabin, Phys. Rev. E **55**, 778 (1997).
[9] E. B. Sirota, X. Z. Wu, B. M. Ocko, and M. Deutsch, Phys. Rev. Lett. **79**, 531 (1997); A. V. Tkachenko and Y. Rabin, *ibid.* **79**, 532 (1997).
[10] P. K. Mukherjee and M. Deutsch, Phys. Rev. E **61**, 637 (2000).
[11] E. Sloutskin, E. B. Sirota, H. Kraack, B. M. Ocko, and M. Deutsch, Phys. Rev. E **64**, 031708 (2001).
[12] X. Z. Wu, B. M. Ocko, H. Tang, E. B. Sirota, S. K. Sinha, and M. Deutsch, Phys. Rev. Lett. **75**, 1332 (1995).
[13] X. Z. Wu, A. Doerr, B. M. Ocko, E. B. Sirota, O. Gang, and M. Deutsch, Colloids Surf., A **128**, 63 (1997).
[14] P. G. DeGennes, Rev. Mod. Phys. **57**, 827 (1985); B. M. Law, Prog. Surf. Sci. **66**, 155 (2001); A. J. Liu and M. E. Fisher, Phys. Rev. A **40**, 7202 (1989); J. W. Schmidt and M. R. Moldover, J. Chem. Phys. **99**, 582 (1993); B. M. Law, Phys. Rev. Lett. **69**, 1781 (1992); H. Kellay, D. Bonn, and J. Meunier, *ibid.* **71**, 2607 (1993).
[15] E. B. Sirota, J. Chem. Phys. **112**, 492 (2000).
[16] O. Gang, B. M. Ocko, X. Z. Wu, E. B. Sirota, and M. Deutsch, Phys. Rev. Lett. **80**, 1264 (1998).
[17] E. B. Sirota and X. Z. Wu, J. Chem. Phys. **105**, 7763 (1996).
[18] E. A. Guggenheim, *Mixtures* (Oxford University Press, Oxford, 1952).
[19] E. A. Guggenheim, Proc. R. Soc. London, Ser. A **148**, 304 (1935); J. H. Hildebrand, J. Am. Chem. Soc. **51**, 66 (1929).
[20] M. Deutsch and B. M. Ocko, in *Encyclopedia of Applied Physics*, edited by G. L. Trigg (VCH, New York, 1998), Vol. 23, p. 479.
[21] H. Kraack, E. B. Sirota, and M. Deutsch, J. Chem. Phys. **112**, 6873 (2000).
[22] A. Guinier, *X-Ray Diffraction* (Freeman, San Francisco, 1963).
[23] E. B. Sirota, H. E. King, D. M. Singer, and H. H. Shao, J. Chem. Phys. **98**, 5809 (1993).
[24] G. L. Gaines, *Insoluble Monolayers at the Liquid–Gas Interface* (Wiley, New York, 1966).
[25] G. Roberts, *Langmuir–Blodgett Films* (Plenum, New York, 1990), p. 108, and references therein.
[26] J. Als-Nielsen and D. McMorrow, *Elements of Modern X-ray Physics* (Wiley, New York, 2001).
[27] Y. Kraftmakher, *Lecture Notes on Equilibrium Point Defects and Thermophysical Properties of Metals* (World Scientific, Singapore, 2000); D. N. Kagan, *Issledovaniya Termodinamicheskih Svoistv Veshestv Metodami Adiabaticheskoy Kalorimetrii* (Akademiya Nauk SSSR, Moscow, 1982).
[28] See the web site of Fairchild Semiconductor at http://www.fairchildsemi.com
[29] E. B. Sirota, D. M. Singer, and H. E. King, J. Chem. Phys. **100**, 1542 (1994).
[30] R. R. Matheson, Jr. and P. Smith, Polymer **26**, 288 (1985).
[31] E. B. Sirota and A. B. Herhold, Science **283**, 529 (1999); E. B. Sirota and A. B. Herhold, Polymer **41**, 8781 (2000).
[32] A. Braslau, P. S. Pershan, G. Swislow, B. M. Ocko, and J. Als-Nielsen, Phys. Rev. A **38**, 2457 (1988); M. K. Sanyal, S. K. Sinha, K. G. Huang, and B. M. Ocko, Phys. Rev. Lett. **66**, 628 (1991); B. M. Ocko, X. Z. Wu, E. B. Sirota, S. K. Sinha, and M. Deutsch, *ibid.* **72**, 242 (1994).
[33] B. M. Ocko, E. B. Sirota, M. Deutsch, E. DiMasi, S. Coburn, J. Strzalka, S. Zheng, A. Tronin, T. Gog, and C. Venkataraman, Phys. Rev. E **63**, 032602 (2001).
[34] L. E. Reichl, *A Modern Course in Statistical Physics* (University of Texas, Arlington, 1980).
[35] R. Defay and I. Prigogine, *Surface Tension and Adsorption* (Wiley, New York, 1966).
[36] P. Flory, *Principles of Polymer Chemistry* (Cornell University Press, Ithaca, 1953).
[37] J. H. Hildebrand and R. L. Scott, *The Solubility of Nonelectrolytes* (Reinhold, New York, 1950).
[38] See Ref. 18, p. 23.
[39] E. Sloutskin *et al.* (unpublished).
[40] S. S. Katti and S. Pathak, J. Chem. Eng. Data **14**, 73 (1969).